



Deposited via The University of Sheffield.

White Rose Research Online URL for this paper:

<https://eprints.whiterose.ac.uk/id/eprint/233455/>

Version: Published Version

---

**Article:**

Lai, Y., Liu, X., Davies, M. et al. (2024) Characterisation of wood combustion and emission under varying moisture contents using multiple imaging techniques. *Fuel*, 373. 132397. ISSN: 0016-2361

<https://doi.org/10.1016/j.fuel.2024.132397>

---

**Reuse**

This article is distributed under the terms of the Creative Commons Attribution-NonCommercial-NoDerivs (CC BY-NC-ND) licence. This licence only allows you to download this work and share it with others as long as you credit the authors, but you can't change the article in any way or use it commercially. More information and the full terms of the licence here: <https://creativecommons.org/licenses/>

**Takedown**

If you consider content in White Rose Research Online to be in breach of UK law, please notify us by emailing [eprints@whiterose.ac.uk](mailto:eprints@whiterose.ac.uk) including the URL of the record and the reason for the withdrawal request.



## Full Length Article

# Characterisation of wood combustion and emission under varying moisture contents using multiple imaging techniques

Yufeng Lai<sup>a</sup>, Xuanqi Liu<sup>b,c,\*</sup>, Matthew Davies<sup>a</sup>, Callum Fisk<sup>a</sup>, Michael Holliday<sup>a</sup>, David King<sup>d</sup>, Yang Zhang<sup>e</sup>, Jon Willmott<sup>a,\*\*</sup>

<sup>a</sup> Department of Electronic and Electrical Engineering, The University of Sheffield, Sheffield S1 4ET, United Kingdom

<sup>b</sup> School of Low-Carbon Energy and Power Engineering, China University of Mining and Technology, Xuzhou 221116, China

<sup>c</sup> Research Centre for Smart Energy, China University of Mining and Technology, Xuzhou 221116, China

<sup>d</sup> Advanced Manufacturing Research Centre, the University of Sheffield, Rotherham S60 5TZ, United Kingdom

<sup>e</sup> Department of Mechanical Engineering, The University of Sheffield, Sheffield S1 3JD, United Kingdom



## ARTICLE INFO

## Keywords:

Wood combustion  
Multiple imaging system  
MWIR hyperspectral imaging  
LWIR thermal imaging  
Moisture content  
Combustion dynamics

## ABSTRACT

In this study, the complex combustion process of natural wood, with different moisture contents, has been characterised using a pioneering approach that integrated Mid-Wavelength Infrared (MWIR) Hyperspectral Imaging (HSI), Schlieren imaging, Long-Wavelength Infrared (LWIR) thermal imaging and visual imaging. The experiment involved the combustion of oak wood samples with moisture contents varying from dry (defined as 0%) to 30%. This setup enabled a detailed investigation into the combustion process, examining aspects such as weight loss rates, thermal behaviours, spectral radiance of gas emissions and flow structures. Higher wood moisture levels were associated with decreased fuel consumption and sustainability of the combustion. The radiance ratios of CH<sub>4</sub>/CO<sub>2</sub> and CO/CO<sub>2</sub> were higher in samples with increased moisture during the initial combustion stages, indicating reduced efficiency in gas-phase combustion. The different combustion stages: flaming and smouldering, were characterised by the thermal profiles. Results demonstrated the moisture level significantly affected the initiation of both flaming and smouldering combustion, as moisture can suppress the thermal pyrolysis of flammable gases during ignition and the evaporation of the residual water can cool the surface locally after ignition. Additionally, the samples with high moisture content transitioned more quickly and directly to smouldering combustion. This transition is further evidenced by lower emissions of flammable gases and a significant decrease in the intensity gradient of flow structures in high moisture conditions. This comprehensive study highlights the potential of multi-wavelength techniques in combustion research. The findings have significant implications for optimising biomass combustion processes in various applications, contributing to the broader field of energy and combustion science.

## 1. Introduction

Wood combustion is a critical process in various applications, ranging from domestic heating to industrial energy production. Understanding the behaviour of wood combustion, especially under varying moisture conditions, is essential for optimising combustion efficiency and reducing harmful emissions [1,2,3].

Previous research highlighted that higher moisture levels in wood significantly increase energy consumption for moisture evaporation, affecting temperature profiles, emissions, and combustion efficiency

[4–7]. Specifically, studies have demonstrated that high moisture content in wood negatively impacts pyrolysis and greenhouse emissions generation [2] while it typically results in higher particulate emissions factors and increases the time for ignition [8]. Moreover, the simultaneous processes of dehydration, pyrolysis, and combustion in moist wood have been studied, revealing the correlation between thermal degradation rate of biomass pyrolysis and moisture content [9]. It has been observed that while higher temperatures can intensify mass loss rates and the release of flammable gases, the presence of moisture concurrently diminishes the formation of these combustion products

\* Corresponding author at: School of Low-Carbon Energy and Power Engineering, China University of Mining and Technology, Xuzhou 221116, China.

\*\* Corresponding author at: Department of Electronic and Electrical Engineering, The University of Sheffield, Sheffield S1 4ET, United Kingdom.

E-mail addresses: [xuanqi.liu@cumt.edu.cn](mailto:xuanqi.liu@cumt.edu.cn) (X. Liu), [j.r.willmott@sheffield.ac.uk](mailto:j.r.willmott@sheffield.ac.uk) (J. Willmott).

<https://doi.org/10.1016/j.fuel.2024.132397>

Received 14 May 2024; Received in revised form 25 June 2024; Accepted 30 June 2024

Available online 2 July 2024

0016-2361/© 2024 The Authors. Published by Elsevier Ltd. This is an open access article under the CC BY-NC-ND license (<http://creativecommons.org/licenses/by-nc-nd/4.0/>).

[10,11]. The moisture acts as a heat sink, lowering temperatures and altering the chemical processes involved in wood degradation, which in turn affects the release of volatile compounds and increases char production, leading to the transition to the smouldering combustion [12,13].

While many studies focused on specific aspects of combustion, such as emission factors, thermal efficiency, or pyrolysis, the complex process of biomass fuel combustion requires comprehensive process monitoring. The distribution of gas-phase species can be dynamically influenced by combustion conditions [14]. Conventional gas detection generally collects the combustion products at a specific point or analysed the flue gas, which cannot provide information on spatial distribution or flow conditions [15,16,17,18]. In addition, the dynamics in combustion stages, such as from flaming to smouldering and from dehydration to self-sustained combustion, are related to thermal and flow fields as well as the pyrolysis of flammable gases. Their spatial distribution can provide valuable insights incorporated when synchronised, but current research has not yet achieved this [19,20]. An in-situ, image-based and multi-faceted approach for combustion process monitoring is highly demanded [21].

Our study addresses this gap by integrating multiple imaging techniques, aiming for synchronous observation and analysis of combustion stages, behaviours, and dynamics, providing new insights and enhancing the understanding of wood combustion processes. Synchronised multiple imaging systems benefit in-depth combustion research, especially for the complex biomass combustion [22,23]. A combination of modern imaging techniques such as mid-wavelength

infrared (MWIR) hyperspectral imaging (HSI), long-wavelength infrared (LWIR) thermal imaging and Schlieren imaging would offer a comprehensive understanding of the combustion process. Further benefits can be realised when these are synchronised temporally, spatially and spectrally, allowing detailed characterisation of temperature profiles, emission spectra, and gas-phase dynamics.

This work aims to characterise the complex wood combustion process under varying moisture conditions with overall combustion rate, thermal behaviour examination, spectral radiance analysis, and synchronised visualisations. This study provides a comprehensive view of the combustion process, revealing the interactions between moisture content and combustion dynamics. Importantly, it highlights the transitions between different combustion stages, corresponding with changes in thermal and gas emission profiles and flow structures.

## 2. Methodologies

### 2.1. Experimental arrangement

The experimental setup is illustrated in Fig. 1. The imaging system consisted of four cameras to monitor the combustion process with different methods, as shown in Fig. 1(a). A visual camera was employed to monitor the burning process and assist in identifying the transition from flaming to smouldering. The Schlieren imaging (Photron FAST-CAM SA5) is sensitive to any density change of gas, thus enabling the hot gas flow field surrounding the burning wood to be monitored. This provides insight into water evaporation and gas-phase combustion

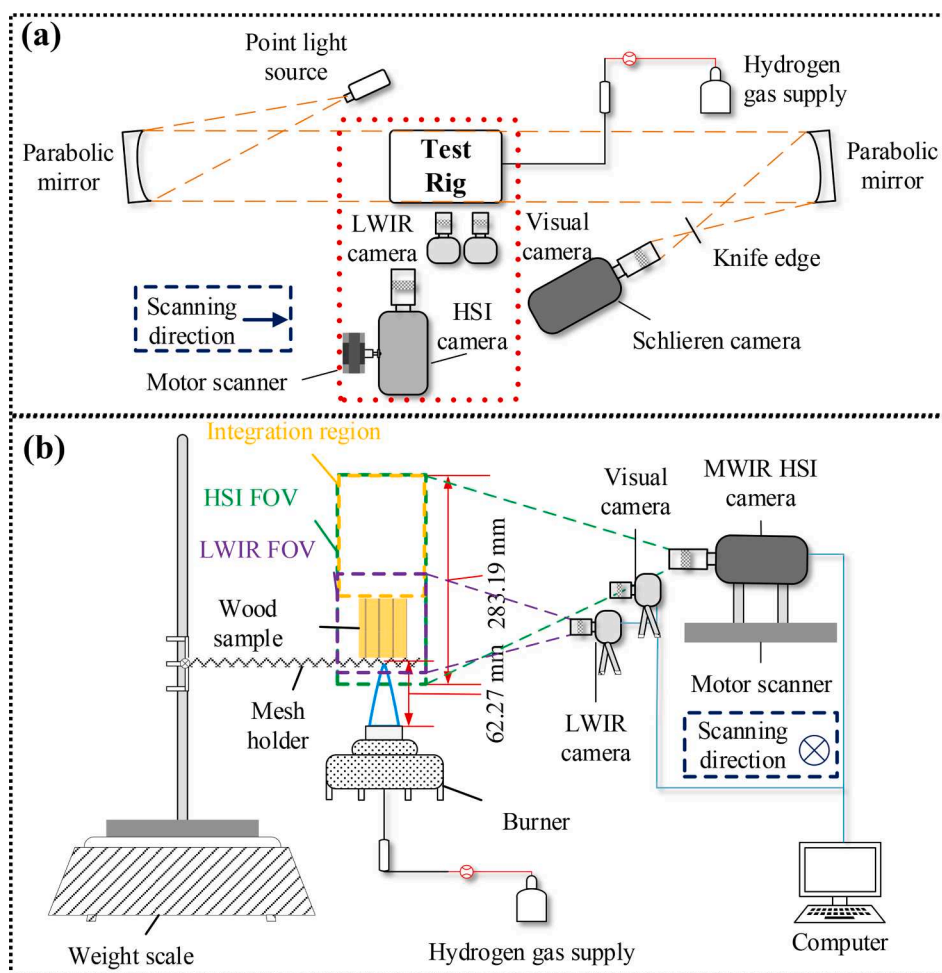


Fig. 1. Experimental arrangements. (a) Imaging systems. (b) Test rig arrangement (the red dotted box in (a)). (For interpretation of the references to colour in this figure legend, the reader is referred to the web version of this article.)

intensity. A LWIR camera (PyrOptik, model LW640) was used to monitor the wood side-surface temperature after pre-calibration. The side surface temperature was used to determine the wood pyrolysis intensity and the effect of water evaporation. A MWIR HSI system (Specim, FX50, 16 bits, 640 pixels spatial resolution) was used to image the emissions of the burning wood. The MWIR HSI camera employed a push-broom scanning method across the burning wood using a translation stage. An image of the scene was cropped by a slit (19.2  $\mu\text{m}$ ) and then dispersed across a MWIR focal plane array. A 3-D data cube was obtained and the HSI was reconstructed after the dark-offset subtraction and image processing [24]. Each scan duration was approximately 10 s, followed by another 10 s for data storage and camera cooling; thus a time averaged HSI of 10 s with 10 s interval was obtained.

### 2.1.1. Test rig arrangement

The test rig is shown in detail in Fig. 1 (b). The wood sample was placed on a mesh holder in order to minimise the effects on the flow field, then the sample holder was placed on an analytical balance (ADAM NBL 84i) with a precision of 0.1 mg to continuously record the weight loss.

A hydrogen burner with a 9.6 mm diameter nozzle was used for igniting the wood sample with a flowrate of 3.0 L/min. Hydrogen fuel was used to ensure that emissions from the pilot flame did not interfere with the carbon-based spectral data obtained from the MWIR HSI system. Each sample was pilot ignited for 40 s, then the fuel supply was cut off and the sample burning was then self-sustained.

The MWIR HSI camera started to record and scan when the wood samples had been pilot ignited for 20 s to measure the emissions during the evaporation/ignition process. Then the camera recorded the emissions every 20 s to measure the significant point in the combustion: when the ignition was just cut off and self-sustained burning.

### 2.1.2. Sample preparation

Natural oak wood was cut into 15 mm  $\times$  15 mm  $\times$  30 mm cuboid samples. The natural wood has anisotropic characteristics including density, grain, and porosity. The anisotropic nature of wood significantly influences moisture transport, representing the different drying speeds, and the dynamic behaviours during drying and water uptake [25,26,27]. This introduced challenges in standardising the moisture content across all samples. Therefore, a set of samples with moisture contents ranging from 8 % to 30 % with very small intervals was prepared, measuring the actual moisture content of each sample to reflect their true conditions. In terms of sample preparation, the present study utilised a water-soak method to obtain varied moisture contents of the wood [28,29]. All the samples were pre-dried for 12 h at 100  $^{\circ}\text{C}$  then the weight was measured as an analogue for moisture content being at 0 % in this study. Then, the dried samples were submerged inside a distilled water tank for 4–10 h to obtain various water contents compared with the control group. After all the samples achieved the required moisture contents, they were set in vacuum for 48 h, to ensure uniformity of internal moisture.

It should be noticed that the procedures used in the present work did not completely remove the natural moisture in the wood samples. Wood contains various types of moisture, including free water, weakly bound water, and strongly bound water [30,26]. Free water, located in the cell lumens and intercellular spaces, evaporates quickly during drying, while weakly bound water, held by capillary forces within the cell walls, evaporates more gradually. Strongly bound water is chemically bonded to the cellulose and hemicellulose in the wood and is released slowly during the drying process.

The sample preparation procedures tended to remove the water that is loosely associated with the wood, and reintroduce the free and weakly bound water for a comparable experiment across various moisture contents. Although the reintroduced water did not completely replicate the naturally humidified state because the submerging process cannot perfectly reverse the pathway that the moisture banded in the

microstructures, this approach ensures the representative to the industrial drying practices of biomass fuels.

## 2.2. Calibrations

### 2.2.1. Spectral radiance

The nonuniform spectral response of the MWIR HSI camera needs to be calibrated to determine the actual spectral radiance emitted by different species [31]. The calibration was conducted by scanning and capturing images of a blackbody furnace (emissivity  $\sim 0.99$ ) in the temperature range from 350  $^{\circ}\text{C}$  to 800  $^{\circ}\text{C}$ , in 50  $^{\circ}\text{C}$  increments. The blackbody radiation within the cameras spectral range can be calculated as Eq. (1):

$$B(\lambda, T) = \frac{(2hc^2)^*}{\lambda^5} \frac{1}{e^{hc/\lambda kT} - 1} \quad (1)$$

where  $B(\lambda, T)$  is the blackbody radiation,  $h$  is Planck's constant,  $c$  is the speed of light,  $\lambda$  is the wavelength,

$k$  is Boltzmann's constant,  $T$  is the absolute temperature.

The digital level ( $DL(\lambda, T)$ ) can be obtained after subtracting the offset from zero digital-logic-levels spectrally at different temperatures. The calibration factor  $F$  can be obtained by calculating the ratios between the spectral radiance and the digital level, shown as Eq. (2):

$$F(\lambda, T) = \frac{DL(\lambda, T)}{B(\lambda, T)} \quad (2)$$

The results of the calibration factor at different temperatures are shown in Fig. 2 (a). The calibration factor was found to be relatively consistent at different temperatures, which means  $F(\lambda, T)$  is less dependent on the temperature. The calibration factors were then spectrally averaged, and the spectral radiance  $I(\lambda, T)$  was calculated as Eq. (3):

$$I(\lambda, T) = DL(\lambda, T)/\bar{F}(\lambda). \quad (3)$$

The field-of-view (FOV) and width-height ratio of the HSI camera was calibrated by scanning a 25 mm aperture placed in front of the blackbody furnace. After reconstructing the images, the width-height ratio of the HSI was measured as 40:1, which was used for reconstructing the images with correct spatial geometry.

### 2.2.2. Thermal radiance

The LWIR camera used in the present study had a spectral range of 7.5–13.5  $\mu\text{m}$ . Its sensitivity to low temperatures benefited the monitoring of the wood temperature under evaporation. The camera has a 640  $\times$  512 pixel resolution, with a fixed framerate of 9 Hz. The calibration was based on Planck's law [32], using a blackbody furnace (emissivity  $\sim 0.99$ ) set from 50  $^{\circ}\text{C}$  to 650  $^{\circ}\text{C}$ . The deviation between the camera-calculated temperature and the actual temperature of the blackbody furnace was quantified as the uncertainty of the calibration. The results of the calibration and the deviation are shown in Fig. 2 (b). The deviation was under 10  $^{\circ}\text{C}$  across the temperature range.

### 2.2.3. Spectral calibrations

Wood combustion is a complex process involving pyrolysis, gas-phase flaming, solid-phase combustion and smouldering combustion [33]. There are typical gas species produced from wood combustion which radiate in the MWIR region, such as volatile organic compounds (VOCs), CO, CO<sub>2</sub>, H<sub>2</sub>O vapour, and NO. Considering CH<sub>4</sub> is the dominant VOC in the biomass pyrolysis process [34], it has been used to represent the VOCs produced from the pyrolysis in the present study. A typical spectrum of the burnt gases of the wood sample is presented in Fig. 2 (c) and (d). The spectral range of the HSI camera was calibrated by the manufacturer in the range of 2707.9 nm–5278.6 nm, in 308 channels. The emission bands of H<sub>2</sub>O, CH<sub>4</sub>, CO<sub>2</sub>, CO and NO were identified using the HITRAN database [35]. It should be noted that there was overlap between the CO<sub>2</sub> and CO bands boundary. The boundary has been

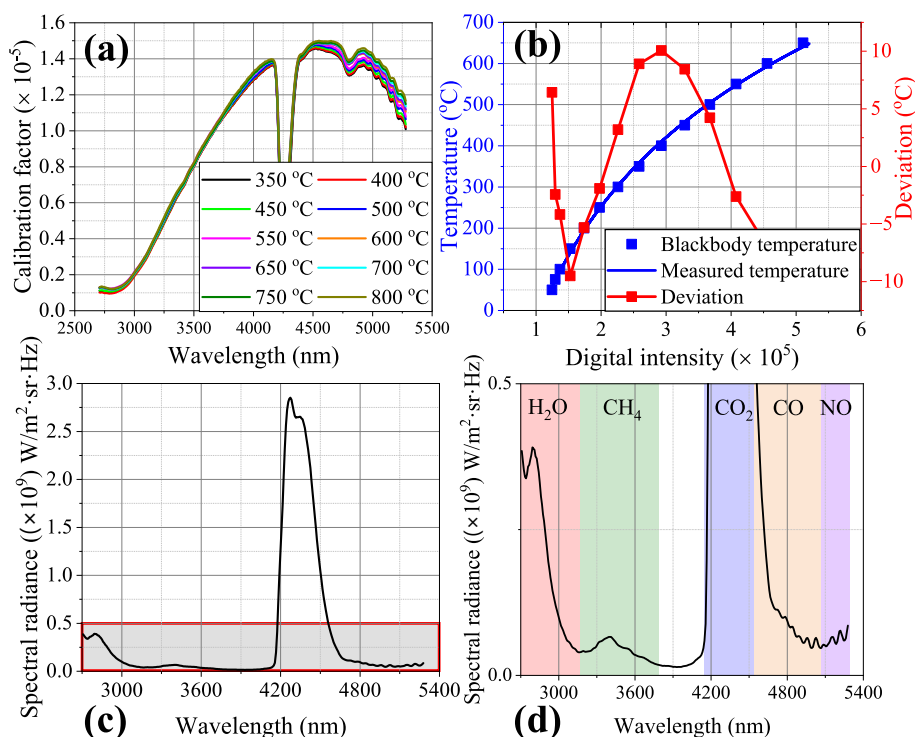


**Fig. 2.** System calibration graphs. (a) Spectral radiance calibration for the MWIR HSI camera. (b) Thermal camera calibration. (c) Example spectrum of the wood gas emission. (d) Gas species identifications based on HITRAN database.

determined between these as the lowest spectral intensity wavelength of  $\text{CO}_2$  reported in HITRAN database which limited effects of overlap on the present results; the effects of the overlap were then negligible.

### 2.3. Data processing

The measured weight loss shows the total fuel consumed and the volume of thermal pyrolysis, which directly reflected the combustion rate. The weight loss was recorded temporally from the time pilot ignition was cut off. For consistency, the data was normalised based on initial sample weight. In addition, the residual weight, representing the remaining fuel sample weight after extinguishment, was measured at the end of self-sustained burning and compared across samples in relation to moisture content.

The side surface temperature of the wood was quantified by averaging the pixel values within the region of interest. The time evolution of average temperature was compared in relation to varying moisture content levels. Furthermore, the peak temperature, which reflects the highest average temperature the wood can reach, and the flame-out temperature, marked by the temperature just before a significant drop, have been quantified against different moisture contents. The surface temperature can also be an indicator of the extinguishment of the wood since most of the thermal pyrolysis ends below  $200\text{ }^\circ\text{C}$  [13,36]. Therefore, the time duration from the pilot ignition to the point when the average temperature fell below  $200\text{ }^\circ\text{C}$  was considered as the burning lifetime of the wood. Similarly, the duration from ignition off to the flame-out point was quantified as the active flaming period, and from flame-out to the end of pyrolysis was considered the smouldering-dominated period.

The spectral results captured by HSI were integrated spatially above the burning wood, shown in the yellow box in Fig. 1 (b). The spectral radiance of each gas species was then integrated spectrally, according to their emission bands shown in Fig. 2 (d). This work utilised a ratio method to estimate the relative change in gas species [37]. The ratio of the spectral radiance emitted by two gas species is related to the relative radiation intensity of the two species. According to Beer-Lambert's Law

that the temperature, pressure and chemical species determine the intensity and shape of individual spectral peaks. It can be assumed that the different gas species are in thermal equilibrium and have same pressure at the same location. Therefore, while the spectral radiance ratios do not directly measure the true ratios of the gas concentrations, they act as indicators for the relative change in gas species, offering comparable results. In this work, three different ratios were utilised to represent the combustion process:  $\text{H}_2\text{O}\%$ , which was obtained by calculating the  $\text{H}_2\text{O}$  spectral radiance percentage against the five major identified species, shown in Fig. 2 (d), indicating the water vapour emission intensity of the gas;  $\text{CH}_4/\text{CO}_2$ , which represented the consumption rate of the flammable pyrolysis product; and  $\text{CO}/\text{CO}_2$ , a direct indicator of the combustion completeness. The HSI results were recorded from the 20 s of pilot ignition with about 10 s interval. The results were presented temporally and the first three time points:  $-20\text{ s}$ ,  $0\text{ s}$  and  $20\text{ s}$  are presented against the moisture content, to show the emission ratios at igniting, ignition off and self-sustained stages.

The HSI images were reconstructed and integrated spectrally along each gas species, then presented with a colourmap after normalisation. It is worth noting that the spectral radiance did not directly reflect the concentration of gas species, because of temperature dependence. However, the HSI could provide insights into the gas distributions and relative intensity, especially in conjunction with Schlieren images.

The Schlieren images represent the thermal gradient of the gas-phase flow, the complexity and contrast refer the more complicated temperature distribution and disturbance level of the flow [38]. The time-averaged mean gradients were adopted to characterise the flow field around the burning wood under varied moisture conditions. 20 images at certain time points (igniting, ignition off and self-sustained) were averaged and calculated using the Prewitt method to show the difference in the inhomogeneities level.

### 2.4. Uncertainty analysis

Given the challenge in repeating the tests at the exact same moisture contents due to the anisotropic nature of wood, the present study

ensured the repeatability of results by conducting the experiments using samples with very small intervals of moisture (typically from 0.05 % to 0.5 % for most cases) in the range from 8 % to 30 %. The quantitative results are presented as trends against moisture content, demonstrating both the repeatability and general trends.

In addition, the tested samples were grouped with closed moisture contents ( $\pm 0.5$  %) at 10 %, 15 %, 20 %, 25 %, 30 % and the control group (0 %), considering the limited differences in combustion behaviours impacted by such small amounts of water. The quantitative results have been averaged within these groups, and the standard deviation has been provided to present the experimental uncertainties.

### 3. Results and discussions

#### 3.1. Overall combustion behaviours

The combustion rate and efficiency of wood is significantly influenced by its moisture content [39,5], which can be directly assessed through the rate of weight loss during burning. Moisture content acts as a critical parameter, affecting both the energy required for evaporation and the subsequent combustion process.

The initial moisture content of the wood samples used which ranges from 8 % to 30 %, with the control case at 0 %. Fig. 3(a) illustrates that residual weight percentage increased with higher sample moisture content. The  $\pm 0.5$  % grouped results in Fig. 3 (b) present a clear increasing trend. This shows that samples with higher moisture content tended to leave a greater proportion of unburnt material, which indicates a lower fuel consumption. Less heat in high moisture sample was available to break down the wood's solid components into combustible gases, leading to more unburned material being left behind [2]. Although the dehydration and thermal pyrolysis occurred simultaneously, the evaporation of water was the dominant process during

ignition [40]. The energy required for water evaporation slows down the rate of thermal degradation of wood, resulting in a slower fuel consumption rate [12].

Fig. 3(c) shows the time evolution of the weight loss rate of typical moisture levels samples. The duration represents the wood combustion process from piloted ignition to extinguishment, as identified by both thermal imaging and the cessation of weight loss. The wood combustion process consisted of dehydration, pyrolysis, and flaming/smouldering [41]. It is found that the weight loss rate was rapid initially for all the samples, indicative of intense flaming combustion, where higher temperatures facilitated rapid pyrolysis and gas release [42]. The weight loss rates slowed as the combustion progressed, transitioning to smouldering-dominated combustion. It was observed that samples with lower moisture exhibited a more rapid weight loss rate and a delayed transition to smouldering combustion. Drier wood can sustain a longer flaming stage because it maintains a high rate of pyrolysis when exposed to sufficient heat [2] while energy in moister samples was consumed for evaporation, shifting the thermal equilibrium. This shift potentially favours char formation and alters the combustion pathway [20].

#### 3.2. Thermal behaviours

The thermal behaviour of wood during combustion is a critical aspect of understanding its burning characteristics as the fuel temperature directly corresponds to the transitions between combustion stages. Fig. 4 (a) presents the temporal evolution of the side surface temperature for wood samples with varying moisture content. The thermal profiles represent different stages of wood combustion: piloted ignition; flaming combustion, where the fuel was sustained at a high-temperature plateau due intense heat release [5]; flaming-smouldering transition, where the fuel temperature began to significantly drop; and the smouldering-dominated combustion, indicating a slower, more moderate solid-

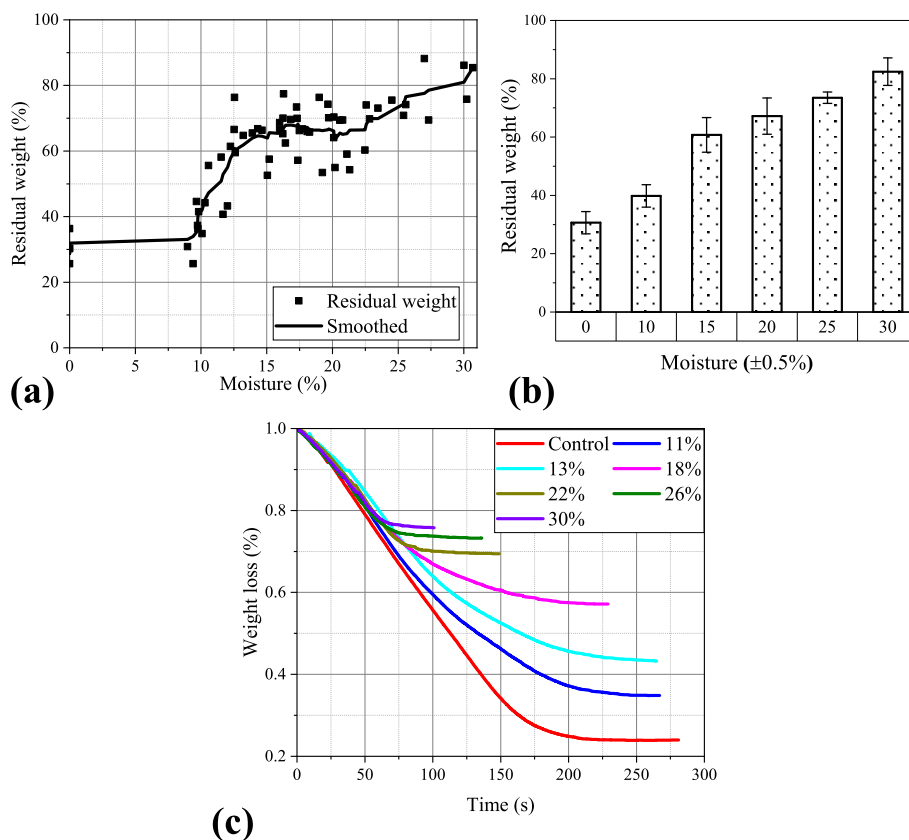


Fig. 3. Moisture content and weight loss. (a) Moisture contents and their residual weight. (b) Averaged residual weight within  $\pm 0.5$  % grouped cases and standard deviation. (c) Time evolution of weight loss rate under typical moisture contents.

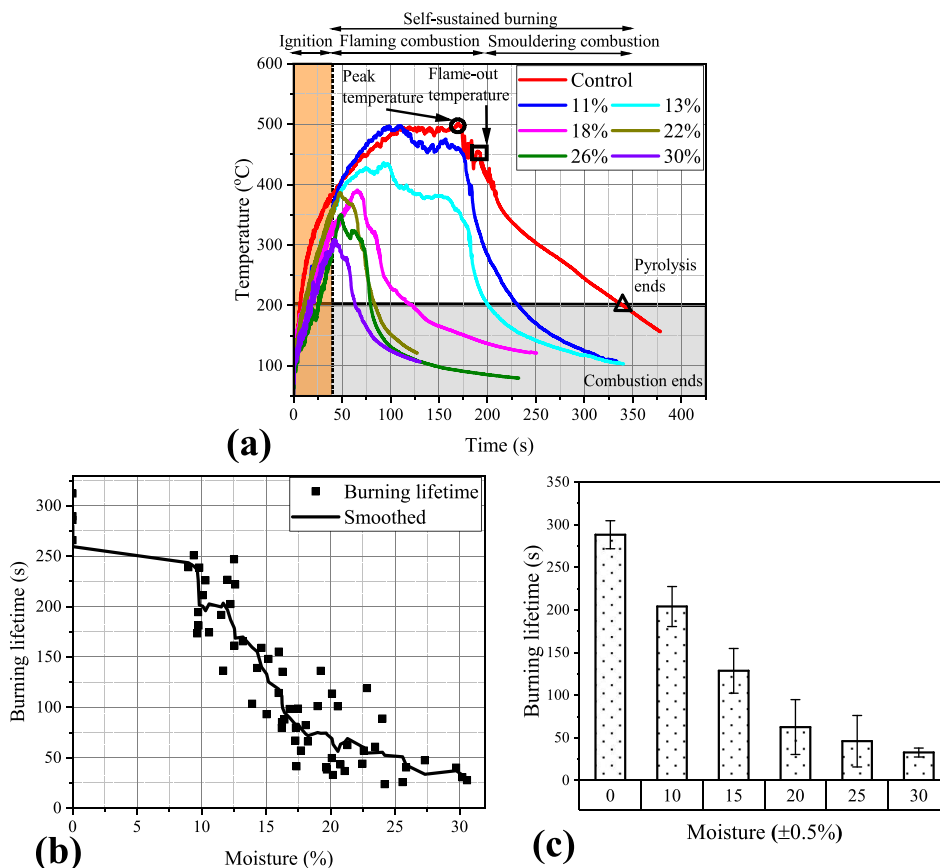


Fig. 4. (a) Time evolution of thermal profiles. (b) Self-sustained burning lifetime. (c) Averaged burning lifetime within  $\pm 0.5\%$  grouped cases and standard deviation.

phase combustion [6]. Fig. 4 (a) shows that the surface temperature has insignificant difference after the piloted ignition was turned off though the lower moisture samples raised the surface temperature more rapidly during the ignition. This represents the moisture has been removed from the exterior surface. During the self-sustained burning, the results illustrate that samples with higher moisture content tended to reach their peak temperature more rapidly, yet these peak temperatures were lower compared to drier samples. This was likely due to the migration of the residual water to the exterior surface and cooled the wood locally with evaporation, subsequently impeded the combustion. Moreover, the duration for which the samples maintained a high-temperature plateau (flaming combustion) was inversely proportional to the moisture content. A temperature threshold of 200 °C was set to represent the extinguish point where at below the rapid pyrolysis of wood ended [13]. Therefore, the burning life for the self-sustained burning can be quantified, as shown in Fig. 4(b). The averaged lifetime within the grouped moisture and their standard deviation are presented in Fig. 4 (c). The results suggest the higher moisture level can lead to a lower ability of self-sustained combustion, and the wood was unable to maintain the necessary thermal conditions for ongoing combustion, resulting in incomplete fuel consumption.

Fig. 5 illustrates the synchronised visual and thermal images of typical moisture samples at various combustion stages that were categorised in thermal profiles. The combustion stages can be also identified based on visible flame presence: flaming (when intense flames exist), transition (characterised by surrounding intense flame-out), and smouldering-dominated combustion. Notably, the low moisture samples exhibit a partial transition to smouldering, where flaming and smouldering coexist, indicating that the temperature remains sufficiently high to sustain the pyrolysis of gas-phase fuels with the combustion proceeded. The thermal images reveal a homogeneous temperature

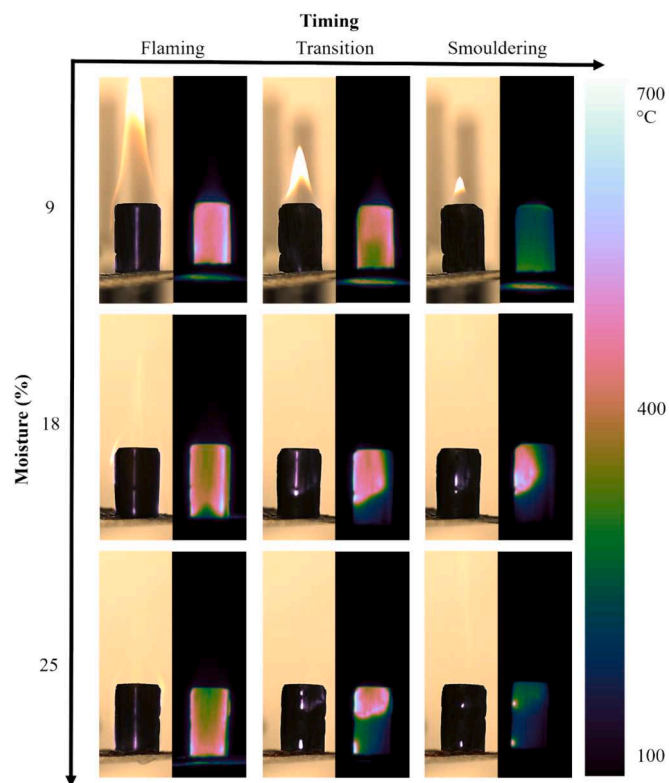


Fig. 5. Example visual and thermal images at critical timings: flaming, transition and smouldering.

distribution across the entire surface of the low moisture samples, in contrast to the high moisture samples, which show only partially heated areas. This phenomenon was due to the residual water migrating from the interior to the exterior through the vessels, subsequently causing localised cooling from the evaporation [43]. Given the larger amount of the bound water residual in high moisture samples [30], the pyrolysis and combustion processes broke the internal microstructures and accelerate the migration of these residual moisture. The evaporation of migrated water partly cooled the surface, leading less fuel involved in the decomposition process, which accelerates the transition from flaming to smouldering combustion [33].

According to the thermal profiles in Fig. 4 (a), high-moisture samples reached peak temperature sooner, close to the end of piloted ignition, indicating a weak initiation of flaming combustion. Although the surface temperatures of high-moisture samples were insignificantly different from those of the drier samples immediately after ignition, considerable heat was consumed in evaporating the residual water that migrated from within, weakening the initiation of the flaming combustion. Gas-phase combustion was a significant contributor for heat release and maintaining a high-temperature plateau. The high-moisture samples have limited heat input from the flaming combustion, shown as the shorter plateau of high temperature compared with drier samples. In detail, Fig. 6 (a) shows the quantitative results of the flaming combustion duration alongside the peak average surface temperature with their averaged value and standard deviation shown in Fig. 6(b). A shorter flaming duration correlated with a lower peak temperature in high moisture samples, indicating that the intensity of flaming combustion is reduced at these higher moisture levels. The endothermic process of water evaporation affected the rate of pyrolysis and the subsequent gas-phase combustion [44]. The lower temperature ( $<320^\circ\text{C}$ ) after initial ignition of the moist samples and the locally cooling from the residual water impeded the rapid pyrolysis generating the flammable gases [13], resulting in a less availability of combustible volatiles from the pyrolysis. Consequently, the gas-phase combustion was suppressed, further

limiting the heat release and thus the potential for sustained high-temperature conditions [2].

Similarly, the smouldering combustion and the flame-out temperature were quantified and presented in Fig. 6 (c) and (d). Wetter samples have a lower flame-out temperature and a correspondingly shorter smouldering combustion duration, indicating a lower ability for self-sustained burning and a greater tendency for the combustion process to cease. Higher moisture content in wood leads to a weaker initiation of smouldering combustion, as evidenced by the lower flame-out temperature. Smouldering combustion, which involves the low-temperature oxidation of the char, requiring higher temperatures for initiation compared to volatile matter [45]. Lower flame-out temperatures in wetter samples indicate the reduced initiation of the char combustion, which is critical for maintaining self-sustained burning. Kinetic studies have reported that the activation energy required for char combustion is higher, making it more sensitive to temperature reductions caused by moisture [46]. Additionally, the lower flame-out temperature reflected a quicker transition from flaming to smouldering combustion due to less pyrolysis of the gas volatiles [5,47] and the cooling effects from the evaporation of residual moisture that migrated to the surface, aligning with the observation of Fig. 5. The low flame-out temperature also indicated the flaming-smouldering transition was induced by the surface cooling rather than by the consumption of the fuel in drier samples, resulting in a high level of incomplete fuel consumption.

### 3.3. Gas emission behaviours

The thermal profiles provide insights in the effects of moisture levels on the different combustion stages: piloted ignition, flaming and smouldering. The intensity and duration strongly depended on the initiation of self-sustained burning, which was determined by the concentration of volatiles from thermal pyrolysis [48] and the conversion of these volatiles to  $\text{CO}_2$  [16,49]. The spectral radiance analysis provides a quantitative analysis of the emissions intensity during wood burning.

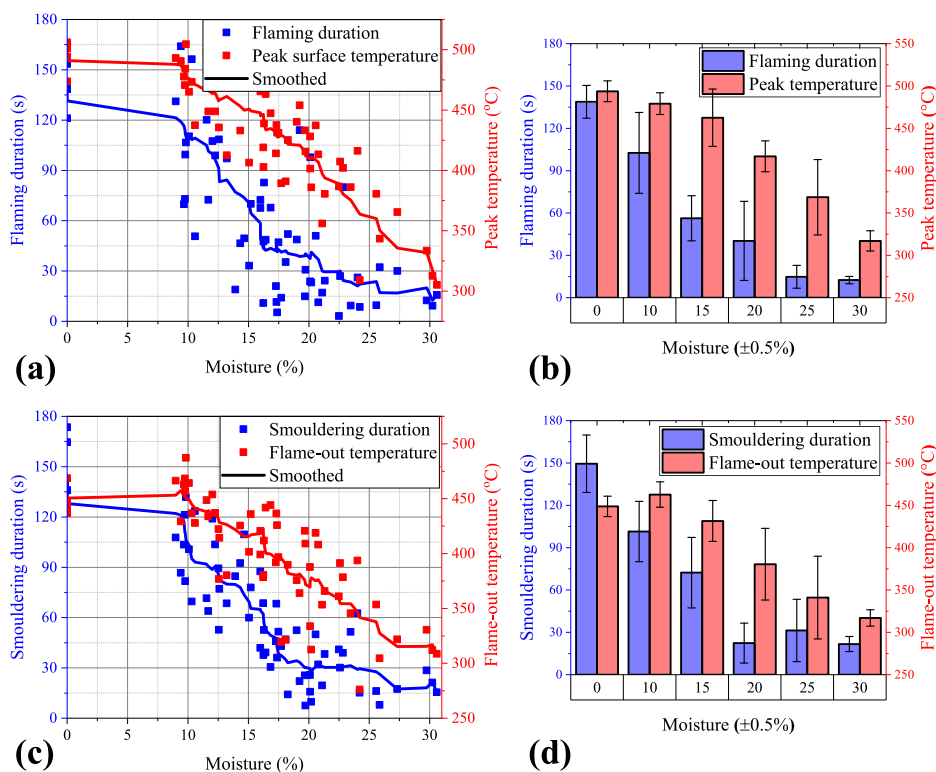


**Fig. 6.** Different combustion stages and corresponding thermal profiles. (a) Flaming combustion. (b). Averaged flaming combustion results within  $\pm 0.5\%$  grouped cases and standard deviation. (c) Smouldering combustion. (d). Averaged smouldering combustion results within  $\pm 0.5\%$  grouped cases and standard deviation.

The radiance ratios of key combustion products, such as  $\text{CH}_4/\text{CO}_2$  and  $\text{CO}/\text{CO}_2$ , can be used as indicators of the combustion efficiency and the completeness of combustion [18,11].

Fig. 7 presents the temporal evolution of key spectral radiance ratios with varied moisture contents. Fig. 7(a) shows that the spectral radiance from water vapour was proportional to the moisture content within the wood samples, which aligned with expected concentration of water vapour in the air. Notably, water emission remained relatively high when the piloted ignition was turned off, especially for the high-moisture samples. This indicates that residual water was still present inside the wood due to incomplete dehydration, although the surface appeared dry and was at a high temperature. It is found that the  $\text{H}_2\text{O}\%$  declined after around 20 s post-ignition, suggesting a stabilisation phase following an initial dehydration phase (from -20 s to 20 s post-ignition). This trend reflects the progressive evaporation of moisture from the wood, which acted as a preliminary procedure before the intensive

combustion occurred. Therefore, the two stages: dehydration and self-sustained, can be characterised in the emission analysis, distinguishing from the combustion stages categorised based on the thermal profiles.

Fig. 7(b) and (c) reveal similar trends, where higher moisture contents corresponded to higher  $\text{CH}_4/\text{CO}_2$  and  $\text{CO}/\text{CO}_2$  ratios.  $\text{CH}_4$  and  $\text{CO}$  are both products from the pyrolysis of biomass fuels [11,50,51]. The higher ratios against  $\text{CO}_2$  were indicative of incomplete combustion, because they indicated a relative increase in the production of unburnt hydrocarbons and incomplete oxidation products, leading to a low intensity of flaming combustion [49] which was aligned with the analysis of thermal profiles. It is found that the low moisture content samples (Control, 9% and 13%) showed the lowest  $\text{CH}_4/\text{CO}_2$  and  $\text{CO}/\text{CO}_2$  ratios during the dehydration stage and maintained similar ratios in the self-sustained burning stage. This indicated that the flammable gases were effectively oxidised and that intensive gas-phase combustion occurred simultaneously with the water evaporation. And the simultaneous

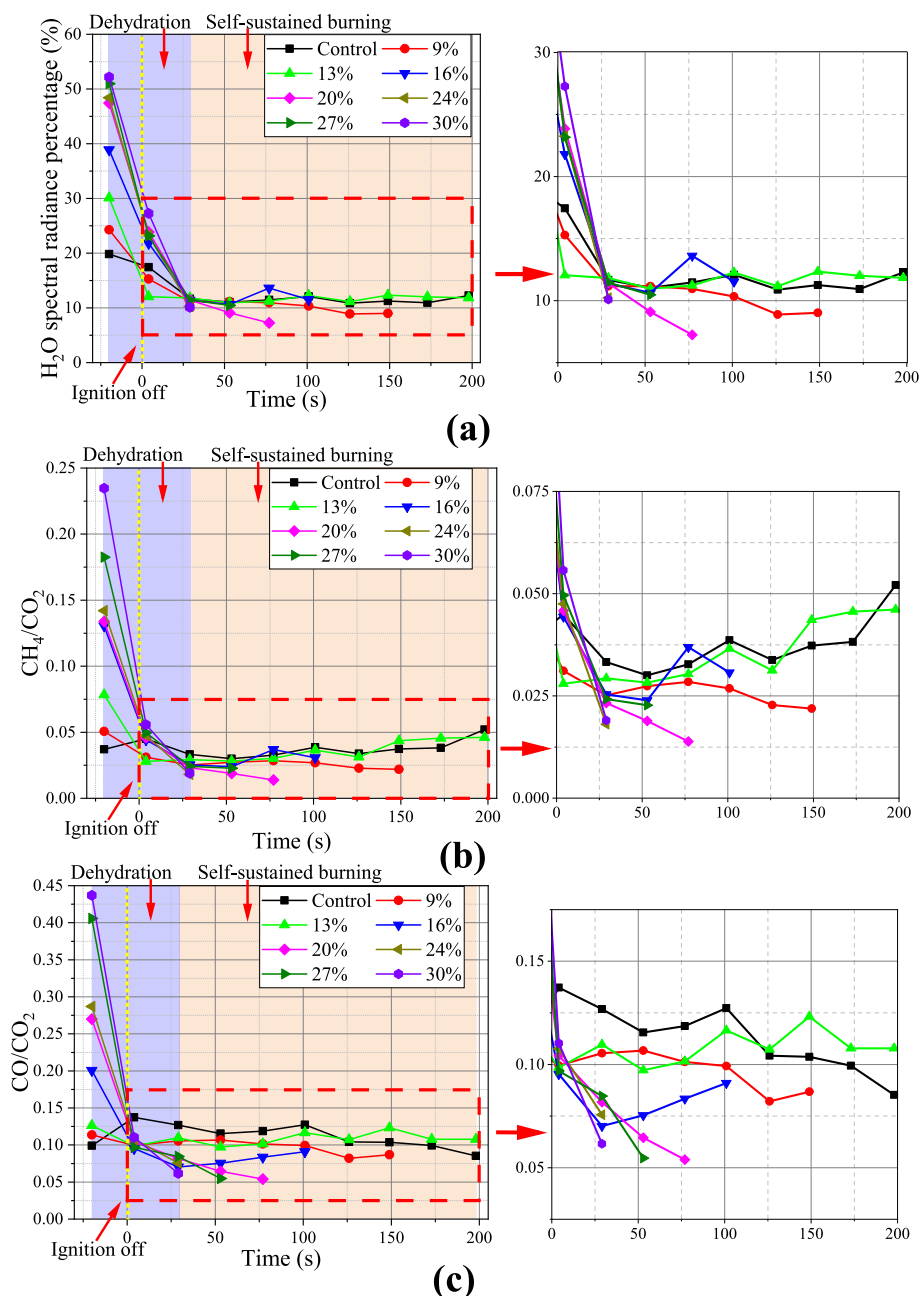


Fig. 7. Time evolution of the spectral radiance ratios. (a)  $\text{H}_2\text{O}\%$ . (b)  $\text{CH}_4/\text{CO}_2$ . (c)  $\text{CO}/\text{CO}_2$ .

flaming-smouldering combustion released sufficient heat for the subsequent evaporation and pyrolysis.

Interestingly, in the self-sustained burning stage (from 20 s onwards), lower  $\text{CH}_4/\text{CO}_2$  and  $\text{CO}/\text{CO}_2$  ratios in samples with higher moisture content was found. This phenomenon may imply a decrease in pyrolytic products because of the reduced thermal degradation of wood components at lower temperatures, due to the constant energy consumed in evaporating the residual water (local cooling in Fig. 5). It also indicated a shift in the combustion regime, from a gas-phase dominated process to a smouldering-dominated combustion, in the presence of higher moisture levels [8]. In contrast, the drier samples exhibited a coexistence of flaming and smouldering phases with a larger area of fuel involved in the thermal pyrolysis (Fig. 5), resulting in a high intensity of smouldering initiation, high consumption rates of fuel and a longer lifetime of self-sustaining combustion.

Besides from the time evolution of the emissions in Fig. 7, Fig. 8 illustrates the spectral radiance ratios at the critical initial combustion periods – igniting, ignition off, and the early self-sustained stages to show the moisture-dependent effects.

It can be observed from Fig. 8 (a) that the  $\text{H}_2\text{O}\%$  increased with

moisture content as expected, and the large proportion of the moisture was removed during the ignition stage. The trend against moisture can be seen in Fig. 8 (b) with the averaged  $\text{H}_2\text{O}\%$  within each moisture group. However, when the pilot ignition was turned off, the increase in  $\text{H}_2\text{O}\%$  with moisture content was still present reflecting that residual water within the wood was migrating to the exterior through the vessels [43]. After the majority of moisture was removed, the  $\text{H}_2\text{O}\%$  levels showed a slight decrease in the higher moisture samples. This trend supported the previous findings that less intense gas-phase combustion and fast transition to the smouldering-dominated combustion in wetter samples, as water was considered as one of the main products in gas-phase combustion.

It is found that the  $\text{CH}_4/\text{CO}_2$  (Fig. 8 (c) and (d)) and  $\text{CO}/\text{CO}_2$  (Fig. 8 (e) and (f)) ratios have a similar trend to that observed in  $\text{H}_2\text{O}\%$  during the pilot ignition, implying less complete combustion and reduced combustion efficiency in moister wood. Higher moisture content inhibited the initiation of intense flaming combustion because the constant evaporation of the residual moisture, aligning with the thermal results in Fig. 6 (a) and (b). At the ignition off stage, the near-consistent ratios across different moisture contents suggested a transitional phase

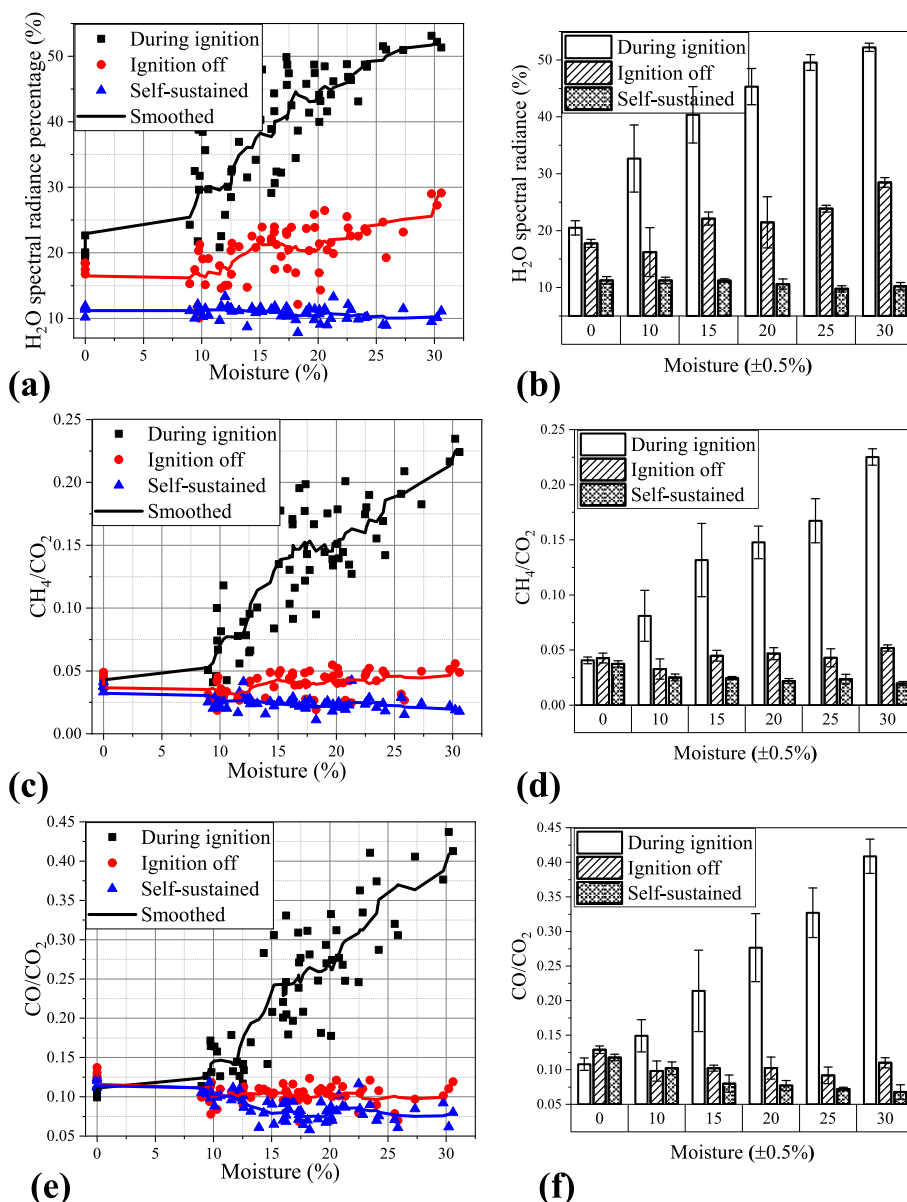


Fig. 8. Spectral radiance ratios during the initial combustion periods. (a)  $\text{H}_2\text{O}\%$ . (c)  $\text{CH}_4/\text{CO}_2$ . (e)  $\text{CO}/\text{CO}_2$ . (b)(d)(f): Group averaged results.

where the high surface temperature from the pilot ignition facilitated the onset of self-sustained burning. However, in the self-sustained burning stage, both  $\text{CH}_4/\text{CO}_2$  and  $\text{CO}/\text{CO}_2$  ratios decreased with increased moisture content, suggesting a suppression of thermal pyrolysis due to lower fuel temperatures. This indicated a reduction in the intensity of gas-phase combustion and rapid transition toward smouldering-dominated combustion in more moist samples since a larger proportion of  $\text{CO}_2$  was generated from the oxidation of solid carbon [8]. The emission profiles provide insights to characterise the flaming-smouldering transition under varying moisture levels, complementing the thermal profile analysis.

### 3.4. Visualisations of flow structure

Visualising the combustion process using multiple imaging techniques is pivotal for a comprehensive understanding of how moisture content influences combustion dynamics and the flow structures. Fig. 9 shows a multi-faceted view by Schlieren, thermal, and HSI images at various moisture levels and combustion stages.

At the ignition stage, the narrowing of the hot gas flow width in higher moisture content samples, observed from Schlieren images, highlighted a diminished intensity of flaming combustion. The heat from the pilot ignition was primarily consumed in evaporating moisture, thus limiting the energy available for triggering the vigorous flaming combustion in the wetter samples. A decrease in surface temperature with

increasing moisture, especially at 18 % and 25 %, indicates a less efficiency of pyrolysis and flaming combustion at this stage. This led to a reduction in the rate of wood degradation, and consequently a lower intensity of gas-phase combustion initiation. The results of lower surface temperature were directly shown in the HIS (Figs. 7 and 8). The diminished  $\text{CH}_4$  and  $\text{CO}_2$  emission intensity in higher moisture samples corroborated the limited pyrolysis and suppressed flaming combustion [2]. Besides, the relative prominence of  $\text{CO}$  emissions compared to  $\text{CO}_2$  suggested the existence of incomplete, smouldering-like combustion [8,52].

When the pilot ignition was turned off, a reduction in the hot gas layer underneath the samples in higher moisture cases was observed in Schlieren images. Previous research indicated that this layer is essential for sustaining biomass combustion since it provided considerable convective heating and flammable gases upwards [22,36]. The lack of a robust convective heating layer in higher moisture samples indicated a weak initiation of the combustion process. Interestingly, the thermal images showed only slightly lower surface temperatures but generally similar temperatures in high-moisture samples compared to low-moisture samples. As previously discussed, the piloted ignition heated the surface, but water still remained inside (Fig. 8(a) and (b)). From HSI, the low moisture samples (0 and 10 %) had intense flame combustion, as the high intensity of  $\text{CO}_2$  emission and sufficient flammable gases for subsequent supply. The gas-phase combustion also occurred for high moisture samples (18 %, 25 %), however, the intensity and efficiency

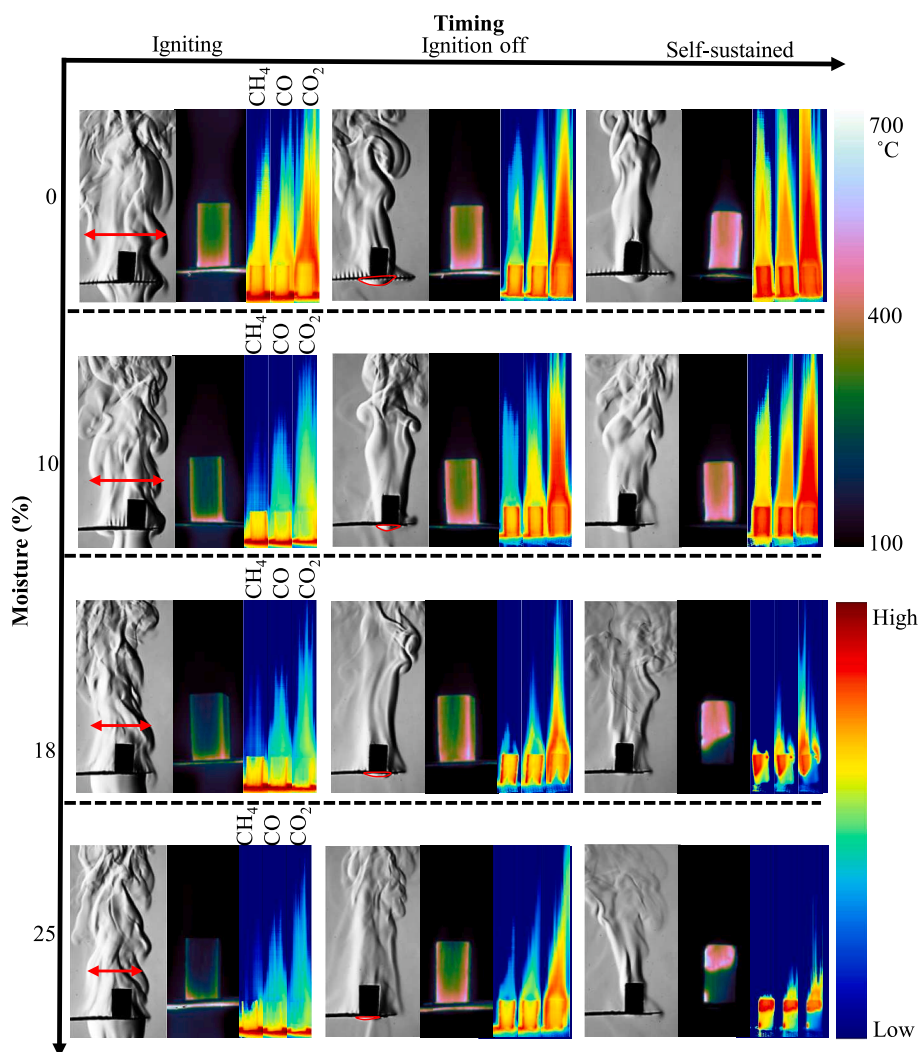


Fig. 9. Visualisations at typical timings and moisture levels.

were lower, reflecting from Schlieren images with less intensity of contrast and gradient level. The low intensity of initiation and the constant energy consumption for the migrated water impeded the subsequent combustion, leading to the fast transition to smouldering combustion.

At the self-sustained burning stage, the flaming combustion in low-moisture samples became stronger than when ignition was just turned off. This was shown in Fig. 4(a) where a larger high-temperature plateau was observed. The dynamic interplay between active flaming combustion and surface heating created a feedback loop that amplified the combustion process and thermal pyrolysis. Intensive emission of flammable gases shown in HSI indicates the existence of a stable anchored flame. The gases from pyrolysis can also be observed in the Schlieren images for 0%–10% moisture samples, suggesting a coexistence of flaming and smouldering phases. Contrarily, significant cooling of the lower half of high moisture samples can be seen in the thermal images, which was attributed to both the evaporation of migrated water and the lack of sufficient hot air flow around the lower surface, resulting in a decreased area under rapid pyrolysis. From the HSI, the low intensity of CO<sub>2</sub> in high moisture samples shows weakened gas-phase combustion. The flammable gases decreased significantly, which related to the decreased ratios in Fig. 8 (c, d) and (e, f) at the self-sustained stage. The concentration of gas emissions near the wood's surface in high moisture samples further indicated the shift from vigorous flaming combustion to a more subdued, smouldering combustion, aligning with the conclusions that the fast transition to the smouldering.

It is observed from the Schlieren images that there is decreased contrast and gradient in the hot gas flow with higher moisture samples. This indicates the significant effect of the moisture on the flow structure [53]. Fig. 10 shows the statistic results of the mean gradient of the flow in Schlieren images at certain time points. The data reveal a decrease in the average gradient with increased moisture levels, representing reduced intensity and complexity in flow structures. During the ignition process, the higher moisture affected the intensity gradient moderately, this was because although the wetter samples exhibited less intensive combustion, the flaming combustion was dominant for all moisture samples. The flow intensity gradient significantly dropped when the piloted ignition was turned off and at the self-sustained burning stage. Such observations align with the visual and thermal profiles discussed earlier, confirming that higher moisture levels expedite the shift from a gas-phase dominated combustion to a smouldering regime, characteristic of less intense thermal activity and slower pyrolysis rates.

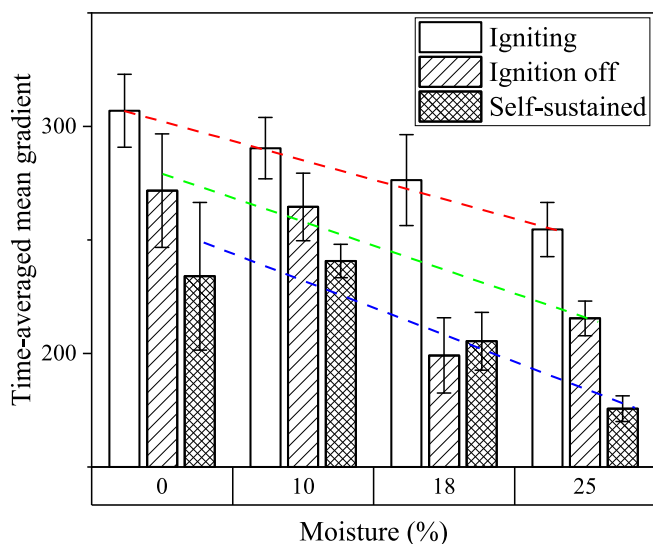


Fig. 10. Time-averaged mean gradient of Schlieren images representing the varied chaos level at certain stages affected by moisture levels.

#### 4. Conclusions

This study presents a comprehensive analysis of wood combustion under varying moisture content. By integrating Mid-Wavelength Infrared (MWIR) Hyperspectral Imaging (HSI), Schlieren imaging, Long-Wavelength Infrared (LWIR) thermal imaging and visual imaging, detailed insights into the complex dynamics of wood combustion have been provided. The key contributions are summarised as follows:

- A clear correlation was observed between moisture content and combustion efficiency, with higher moisture leading to lower weight loss rates and up to 50% increased residual weight compared to dried samples. Furthermore, during the initial combustion stages, the radiance ratios of CH<sub>4</sub>/CO<sub>2</sub> and CO/CO<sub>2</sub> were up to four times higher in samples with increased moisture compared to the control group, indicating reduced efficiency in gas-phase combustion.
- The time evolution of thermal profiles characterised the different combustion stages: flaming and smouldering after the piloted ignition. Drier samples exhibited higher peak temperature (approximately 180 °C difference between 0% and 30% moisture) and extended durations of flaming combustion (up to 120 s difference), indicative of more intense gas-phase combustion. Similarly, higher moisture levels were associated with reduced flame-out temperatures (approximately 150 °C lower) and shorter durations of smouldering combustion (approximately 120 s shorter), suggesting weaker initiation of smouldering in wetter samples.
- Residual water inside was found to be proportional to the moisture level after piloted ignition, as observed by HSI, with up to 30% higher H<sub>2</sub>O spectral radiance emitted by the wet samples compared to the control group. This residual water can migrate to the surface via vessels and locally cool the surface temperature by evaporation.
- Low moisture samples demonstrated a coexistence of flaming and smouldering phases, which supported sustained self-burning. In contrast, samples with high moisture content transitioned more quickly and directly to smouldering combustion, as impeded flaming combustion led to earlier and faster shifts to this less intense combustion stage.
- It was found that higher moisture content leads to lower intensities of flammable gas emissions during the self-sustained combustion stage due to suppressed thermal pyrolysis, accelerating the transition to smouldering combustion. This was supported by a significant decrease in the average intensity gradient of flow with increased moisture at the self-sustained stage, corroborating the dominance of smouldering combustion in wetter samples.

#### CRedit authorship contribution statement

**Yufeng Lai:** Writing – original draft, Visualization, Validation, Software, Methodology, Investigation, Formal analysis, Data curation, Conceptualization. **Xuanqi Liu:** Writing – review & editing, Validation, Methodology, Investigation, Data curation, Conceptualization. **Matthew Davies:** Writing – review & editing, Software, Methodology, Investigation, Conceptualization. **Callum Fisk:** Writing – review & editing, Software, Methodology, Investigation. **Michael Holliday:** Writing – review & editing, Data curation. **David King:** Writing – review & editing, Software, Resources, Methodology. **Yang Zhang:** Writing – original draft, Supervision, Resources. **Jon Willmott:** Writing – review & editing, Supervision, Software, Resources, Project administration, Investigation, Conceptualization.

#### Declaration of competing interest

The authors declare that they have no known competing financial interests or personal relationships that could have appeared to influence the work reported in this paper.

## Data availability

Data will be made available on request.

## References

- Mardones C, Sanhueza L. Tradable permit system for PM<sub>2.5</sub> emissions from residential and industrial sources. *J Environ Manage* 2015;157:326–31. <https://doi.org/10.1016/j.jenvman.2015.03.054>.
- Lee CK, Diehl JR. Combustion of irradiated dry and wet oak. *Combust Flame* 1981;42:123–38.
- Garg P, Wang S, Oakes JM, Bellini C, Gollner MJ. Variations in gaseous and particulate emissions from flaming and smoldering combustion of Douglas fir and lodgepole pine under different fuel moisture conditions. *Combust Flame* 2024;263. <https://doi.org/10.1016/j.combustflame.2024.113386>.
- Dzurenda L, Banski A. The effect of firewood moisture content on the atmospheric thermal load by flue gases emitted by a boiler. *Sustainability (Switzerland)* 2019;11(2). <https://doi.org/10.3390/su11010284>.
- Orasche J, et al. Comparison of emissions from wood combustion. Part 2: Impact of combustion conditions on emission factors and characteristics of particle-bound organic species and polycyclic aromatic hydrocarbon (PAH)-related toxicological potential. *Energy Fuel* 2013;27(3):1482–91. <https://doi.org/10.1021/ef301506h>.
- Bartlett AI, Hadden RM, Bisby LA. A review of factors affecting the burning behaviour of wood for application to tall timber construction. *Fire Technol* 2019;55(1). <https://doi.org/10.1007/s10694-018-0787-y>. Springer New York LLC.
- Sjöström J, Blomqvist P. Direct measurements of thermal properties of wood pellets: elevated temperatures, fine fractions and moisture content. *Fuel* 2014;134:460–6. <https://doi.org/10.1016/j.fuel.2014.05.088>.
- Price-Allison A, et al. The impact of fuelwood moisture content on the emission of gaseous and particulate pollutants from a wood stove. *Combust Sci Technol* 2023;195(1):133–52. <https://doi.org/10.1080/00102202.2021.1938559>.
- Galgano A, Di Blasi C, Ritondale S, Todisco A. Numerical simulation of the glowing combustion of moist wood by means of a front-based model. *Fire Mater* 2014;38(6):639–58. <https://doi.org/10.1002/fam.2203>.
- Fawaz M, Avery A, Onasch TB, Williams LR, Bond TC. Pyrolysis principles explain time-resolved organic aerosol release from biomass burning. *Atmos Chem Phys*.
- Tihay-Felicelli V, Santoni PA, Gerandi G, Barboni T. Smoke emissions due to burning of green waste in the Mediterranean area: Influence of fuel moisture content and fuel mass. *Atmos Environ* 2017;159:92–106. <https://doi.org/10.1016/j.atmosenv.2017.04.002>.
- Chen H, Zhao W, Liu N. Thermal analysis and decomposition kinetics of Chinese forest peat under nitrogen and air atmospheres. *Energy Fuel* 2011;797–803. <https://doi.org/10.1021/ef101155n>.
- Shen DK, Fang MX, Luo ZY, Cen KF. Modeling pyrolysis of wet wood under external heat flux. *Fire Saf J* 2007;42(3):210–7. <https://doi.org/10.1016/j.firesaf.2006.09.001>.
- Saxena SC. Devolatilization and combustion characteristics of coal particles; 1990.
- Kabir E, Kim KH, Ahn JW, Hong OF, Sohn JR. Barbecue charcoal combustion as a potential source of aromatic volatile organic compounds and carbonyls. *J Hazard Mater* 2010;174(1–3):492–9. <https://doi.org/10.1016/j.jhazmat.2009.09.079>.
- Cheng Z, Yang J, Zhou L, Liu Y, Wang Q. Characteristics of charcoal combustion and its effects on iron-ore sintering performance. *Appl Energy* 2016;161:364–74. <https://doi.org/10.1016/j.apenergy.2015.09.095>.
- Huang HL, Lee WMG, Wu FS. Emissions of air pollutants from indoor charcoal barbecue. *J Hazard Mater* 2016;302:198–207. <https://doi.org/10.1016/j.jhazmat.2015.09.048>.
- Deng M, et al. Real-time combustion rate of wood charcoal in the heating fire basin: direct measurement and its correlation to CO emissions. *Environ Pollut* 2019;245:38–45. <https://doi.org/10.1016/j.envpol.2018.10.099>.
- Mello M, Potí B, De Risi A, Passaseo A, Lomascolo M, De Vittorio M. GaN optical system for CO and NO gas detection in the exhaust manifold of combustion engines. *J Opt A Pure Appl Opt* 2006;8(7). <https://doi.org/10.1088/1464-4258/8/7/S38>.
- Zimmermann R, et al. Highly time-resolved imaging of combustion and pyrolysis product concentrations in solid fuel combustion: NO formation in a burning cigarette. *Anal Chem* 2015;87(3):1711–7. <https://doi.org/10.1021/ac503512a>.
- Docquier N, Candel A. Combustion control and sensors: a review. [Online]. Available: [www.elsevier.com/locate/peccs](http://www.elsevier.com/locate/peccs).
- Lai Y, et al. Investigation of forced flow orientations on the burning behaviours of wooden rods using a synchronised multi-imaging system. *Proc Combust Inst* 2022. <https://doi.org/10.1016/j.proci.2022.07.057>.
- Lai Y, Wang X, Rockett TBO, Willmott JR, Zhang Y. Investigation into wind effects on fire spread on inclined wooden rods by multi-spectrum and schlieren imaging. *Fire Saf J* 2022;127. <https://doi.org/10.1016/j.firesaf.2021.103513>.
- Yang H, et al. Experimental and simulated study of the relationship between color camera imaging and color-modeled equivalence ratio measurement. *IEEE Trans Instrum Meas* 2023;72. <https://doi.org/10.1109/TIM.2023.3267359>.
- Gezici-Koç Ö, Erich SJF, Huinink HP, van der Ven LGJ, Adan OCG. Bound and free water distribution in wood during water uptake and drying as measured by 1D magnetic resonance imaging. *Cellulose* 2017;24(2):535–53. <https://doi.org/10.1007/s10570-016-1173-x>.
- Zeng W, Fujimoto T, Inagaki T, Tsuchikawa S, Ma T. Three-dimensional modeling of moisture transport in wood using near-infrared hyperspectral imaging and X-ray computed tomography in conjunction with finite element analysis. *J Wood Sci* 2024;70(1). <https://doi.org/10.1186/s10086-023-02120-2>.
- Ma T, Morita G, Inagaki T, Tsuchikawa S. Moisture transport dynamics in wood during drying studied by long-wave near-infrared hyperspectral imaging. *Cellul* 2022;29(1):133–45. <https://doi.org/10.1007/s10570-021-04290-y>.
- Sargent R. Evaluating dimensional stability in solid wood: a review of current practice. *J Wood Sci* 2019;65(1). <https://doi.org/10.1186/s10086-019-1817-1>. Springer.
- Altgen M, Hofmann T, Militz H. Wood moisture content during the thermal modification process affects the improvement in hygroscopicity of Scots pine sapwood. *Wood Sci Technol* 2016;50(6):1181–95. <https://doi.org/10.1007/s00226-016-0845-x>.
- Ma T, Inagaki T, Tsuchikawa S. Rapidly visualizing the dynamic state of free, weakly, and strongly hydrogen-bonded water with lignocellulosic material during drying by near-infrared hyperspectral imaging. *Cellulose* 2020;27(9):4857–69. <https://doi.org/10.1007/s10570-020-03117-6>.
- Si M, Cheng Q, Zhang Q, Wang D, Luo Z, Lou C. Study of temperature, apparent spectral emissivity, and soot loading of a single burning coal particle using hyper-spectral imaging technique. *Combust Flame* 2019;209:267–77. <https://doi.org/10.1016/j.combustflame.2019.08.003>.
- Lai Y, et al. Investigating the fire-retardant efficiency of intumescent coatings on inclined timber: a study on application strategies and heat transfer mechanisms. *Constr Build Mater* 2023;407. <https://doi.org/10.1016/j.conbuildmat.2023.133586>.
- Haslett SL, et al. Highly-controlled, reproducible measurements of aerosol emissions from African biomass combustion. *Atmos Chem Phys*. doi: 10.5194/acp-2017-679.
- Bertschi IT, Yokelson RJ, Ward DE, Christian TJ, Hao WM. Trace gas emissions from the production and use of domestic biofuels in Zambia measured by open-path Fourier transform infrared spectroscopy. *J Geophys Res: Atmosph* 2003;108(13). <https://doi.org/10.1029/2002jd002158>.
- Rothman LS, et al. The HITRAN2012 molecular spectroscopic database. *J Quant Spectrosc Radiat Transf* 2013;130:4–50. <https://doi.org/10.1016/j.jqsrt.2013.07.002>.
- Lai Y, Wang X, Rockett TBO, Willmott JR, Zhou H, Zhang Y. The effect of preheating on fire propagation on inclined wood by multi-spectrum and schlieren visualisation. *Fire Saf J* 2020;118. <https://doi.org/10.1016/j.firesaf.2020.103223>.
- Thé Riault J, Puckrin E, Lavoie H. Remote monitoring of multi-gas mixtures by passive standoff fourier transform infrared radiometry.
- Liu X, Lai Y, Fisk C, Willmott J, Zhou H, Zhang Y. Experimental investigation on the effects of a mesh in the downstream region of a combustion-driven Rijke tube on self-excited thermoacoustic oscillations. *Exp Therm Fluid Sci* 2024;150. <https://doi.org/10.1016/j.expthermflusc.2023.111061>.
- Price-Allison A, et al. Emissions performance of high moisture wood fuels burned in a residential stove. *Fuel* 2019;239:1038–45. <https://doi.org/10.1016/j.fuel.2018.11.090>.
- Lai Y, et al. Combustion inhibition of biomass charcoal using slaked lime and dolime slurries. *Fire Saf J* 2023;103841. <https://doi.org/10.1016/j.firesaf.2023.103841>.
- Hirata T, Kawamoto S, Nishimoto T. Thermogravimetry of wood treated with water-insoluble retardants and a proposal for development of fire-retardant wood materials. *Fire Mater* 1991;15(1):27–36.
- Shen DK, Fang MX, Luo ZY, Cen KF. Modeling pyrolysis of wet wood under external heat flux. *Fire Saf J* 2007;42(3):210–7. <https://doi.org/10.1016/j.firesaf.2006.09.001>.
- Sedighi Gilani M, Vontobel P, Lehmann E, Carmeliet J, Derome D. Moisture migration in wood under heating measured by thermal neutron radiography. *Exp Heat Transfer* 2014;27(2):160–79. <https://doi.org/10.1080/08916152.2012.757677>.
- Yuen RKK, Yeoh GH, de Vahl Davis G, Leonardi E. Modelling the pyrolysis of wet wood - II. Three-dimensional cone calorimeter simulation. *Int J Heat Mass Transf* 2007;50(21–22):4387–99. <https://doi.org/10.1016/j.ijheatmasstransfer.2007.01.018>.
- Kastanaki E, Vamvuka D. A comparative reactivity and kinetic study on the combustion of coal-biomass char blends. *Fuel* 2006;85(9):1186–93. <https://doi.org/10.1016/j.fuel.2005.11.004>.
- Morin M, Pécate S, Hémati M. Kinetic study of biomass char combustion in a low temperature fluidized bed reactor. *Chem Eng J* 2018;331:265–77. <https://doi.org/10.1016/j.cej.2017.08.063>.
- Mitchell EJS, Lea-Langton AR, Jones JM, Williams A, Layden P, Johnson R. The impact of fuel properties on the emissions from the combustion of biomass and other solid fuels in a fixed bed domestic stove. *Fuel Process Technol* 2016;142:115–23. <https://doi.org/10.1016/j.fuproc.2015.09.031>.
- Fang MX, Shen DK, Li YX, Yu CJ, Luo ZY, Cen KF. Kinetic study on pyrolysis and combustion of wood under different oxygen concentrations by using TG-FTIR analysis. *J Anal Appl Pyrolysis* 2006;77(1):22–7. <https://doi.org/10.1016/j.jaap.2005.12.010>.
- Jimenez J, Farias O, Quiroz R, Yañez J. Emission factors of particulate matter, polycyclic aromatic hydrocarbons, and levoglucosan from wood combustion in south-central Chile. *J Air Waste Manage Assoc* 2017;67(7):806–13. <https://doi.org/10.1080/10962247.2017.1295114>.
- Shi L, Lin Chew MY. Experimental study of carbon monoxide for woods under spontaneous ignition condition. *Fuel* 2012;102:709–15. <https://doi.org/10.1016/j.fuel.2012.06.053>.

- [51] Lee DH, Yang H, Yan R, Liang DT. Prediction of gaseous products from biomass pyrolysis through combined kinetic and thermodynamic simulations. *Fuel* 2007;86(3):410–7. <https://doi.org/10.1016/j.fuel.2006.07.020>.
- [52] Fachinger F, Drewnick F, Gieré R, Borrmann S. How the user can influence particulate emissions from residential wood and pellet stoves: emission factors for different fuels and burning conditions. *Atmos Environ* 2017;158:216–26. <https://doi.org/10.1016/j.atmosenv.2017.03.027>.
- [53] Gubba SR, Ma L, Pourkashanian M, Williams A. Influence of particle shape and internal thermal gradients of biomass particles on pulverised coal/biomass co-fired flames. *Fuel Process Technol* Nov. 2011;92(11):2185–95. <https://doi.org/10.1016/j.fuproc.2011.07.003>.